Studying intact bacterial peptidoglycan by proton-detected NMR spectroscopy at 100 kHz MAS frequency

Catherine M Bougault, Isabel Ayala, Waldemar Vollmer, Jean-Pierre Simorre, Paul Schanda

Studying intact bacterial peptidoglycan by proton-detected NMR spectroscopy at 100 kHz MAS frequency

Catherine Bougault[a], Isabel Ayala[a], Waldemar Vollmer[b], Jean-Pierre Simorre[a], Paul Schanda[a]

[a] *Univ. Grenoble Alpes, CEA, CNRS, Institute for Structural Biology (IBS), 71 avenue des martyrs, 38044 Grenoble, France*
[b] *The Centre for Bacterial Cell Biology, Institute for Cell and Molecular Biosciences, Newcastle University, Richardson Road, Newcastle upon Tyne, NE2 4AX, United Kingdom*

Abstract

The bacterial cell wall is composed of the peptidoglycan (PG), a large polymer that maintains the integrity of the bacterial cell. Due to its multi-gigadalton size, heterogeniety, and dynamics, atomic-resolution studies are inherently complex. Solid-state NMR is an important technique to gain insight into its structure, dynamics and interactions. Here, we explore the possibilities to study the PG with ultra-fast (100 kHz) magic-angle spinning NMR. We demonstrate that highly resolved spectra can be obtained, and show strategies to obtain site-specific resonance assignments and distance information. We also explore the use of proton-proton correlation experiments, thus opening the way for NMR studies of intact cell walls without the need for isotope labeling.

Keywords:
ultra-fast magic-angle spinning, NMR resonance assignment, cell wall, homonuclear correlation experiments

Abbreviations: GlcNAc: *N*-acetylglucosamine (GlcNAc); MurNAc: *N*-acetylmuramic acid; DAP: 2,6-diaminopimelic acid; D-iGlu: D-*iso*glutamic acid;

*Corresponding authors
Email addresses: jean-pierre.simorre@ibs.fr (Jean-Pierre Simorre), paul.schanda@ibs.fr (Paul Schanda)

CP: cross-polarization; INEPT: Insensitive Nuclei Enhanced by Polarization Transfer

Introduction

Magic-angle spinning (MAS) solid-state NMR (ssNMR) spectroscopy has the unique possibility to provide atom-specific insight into (bio-)molecular systems without the need for crystalline or solubilized samples. Over the last 15 years, ssNMR has rapidly grown, and it has enabled the determination of protein structures at atomic resolution, including crystalline proteins (Castellani et al. (2002); Bertini et al. (2010); Huber et al. (2011); Linser et al. (2011a); Knight et al. (2012)), amyloid fibrils (reviewed by Comellas and Rienstra (2013)), membrane proteins (Park et al. (2012); Shahid et al. (2012); Wang et al. (2013a)) and large assemblies (Loquet et al. (2012); Morag et al. (2015); Andreas et al. (2016)). A particularly attractive property of ssNMR is its ability to work with cell membranes (Dick-Perez et al. (2011)), cell walls (Tong et al. (1997); Cegelski et al. (2002, 2010); Wang et al. (2013b); Romaniuk and Cegelski (2015)) or entire cells (Renault et al. (2010, 2012)). The focus of the present manuscript is the bacterial peptidoglycan, a giga-dalton large heteropolymer composed of linear glycan strands composed of two alternating carbohydrates cross-linked through short peptide stems. Unique to bacteria, peptidoglycan biosynthesis and maturation is an important target for antibiotics, and is therefore involved in a multitude of complexes formed with antibiotics, cell wall enzymes, virulence factors and immunity defense systems.

There are numerous open questions related to the structure and dynamics of peptidoglycan, as well as its interactions with other components of the cell wall or biosynthetic and maturation enzymes. While the chemical structure of peptidoglycan is known, the three-dimensional structure of this extended network is hardly understood (Turner et al. (2018); Li et al. (2018); Pazos et al. (2017)) and even more so at atomic resolution. Antibiotics are assumed to impact the peptidoglycan saccharidic chain length and chemical cross-linking, and thereby its structure and dynamics. Both perturbations need to be character-

ized in details in various organisms. In this respect MAS NMR stands out as the sole technique that provides atomic-resolution insight into structural parameters and dynamics of intact peptidoglycan isolated (Tong et al. (1997); Kern et al. (2010)) or in interaction with antibiotics or cell wall components (Tong et al. (1997); Cegelski et al. (2002); Kim et al. (2006, 2008); Kern et al. (2010)). Furthermore, it is known that this network is highly dynamic, and that it is constantly remodeled by hydrolases and polymerizing or cross-linking enzymes (Pazos et al. (2017)).

Despite the obvious importance of peptidoglycan not only for fundamental academic research but also for biomedical applications, complexes between peptidoglycan and biosynthetic or maturation enzymes nevertheless have largely escaped so far the high-resolution characterization by most structural biophysical methods. NMR has the potential to provide structural information, insight into dynamics, and high-resolution models of peptidoglycan:enzyme complexes (Schanda et al. (2014)). The structural NMR information may come from the measurement of inter-atomic distances - ideally long-range distances - or dihedral angles; dynamic information may be obtained from dipolar-coupling or relaxation parameters; finally, interaction studies can be based on the observation of altered NMR parameters in the complex compared to the free components, or direct distance measurements between atoms on peptidoglycan and its binding partners (enzymes, antibiotics). Fundamental to all these NMR approaches is the ability to observe spectra at sufficient sensitivity and resolution. Yet, in NMR studies of complex biomolecular systems, such as peptidoglycan, the primary hurdles often are the limited detection sensitivity, signal overlap and hence limited resolution, as well as difficulties to obtain these biological samples in sufficient quantity with adequate labeling schemes.

Until recently, biomolecular ssNMR studies have been based primarily on the use of ^{13}C-detected experiments at MAS frequencies of < 20 kHz, using sample rotors with diameters of 3.2 – 4 mm and sample quantities of > 20 mg. Obtaining such large amount of sample is often a major bottleneck, but required to achieve sufficient sensitivity in such experiments. Proton-detection

has intrinsically higher sensitivity due to the larger gyromagnetic ratio of ^{1}H spins compared to ^{13}C. However the resulting larger ^{1}H-^{1}H dipolar coupling also gives rise to severe line broadening. For example, at MAS frequencies of 20 kHz, typically employed with 3.2 mm rotors, ^{1}H line widths in fully protonated proteins are of the order of 300-500 Hz (Marchetti et al. (2012)), which generally excludes extraction of site-specific information and resonance assignment.

High-resolution proton-detected ssNMR spectroscopy of biomolecules has become possible through technological advances, namely on the one hand with the introduction of partial deuteration schemes (increasing inter-proton distances and thus decreasing line broadening due to dipolar-dephasing), and on the other hand with the development of hardware allowing for higher MAS frequencies, and thus more efficient averaging of dipolar interactions and smaller line widths. Using deuterated proteins, 100 % back-protonation of the exchangeable amide sites, and MAS frequencies of up to 60 kHz, ^{1}H line widths of ca. 50-100 Hz were obtained (Zhou et al. (2007a); Lewandowski et al. (2011a); Fraga et al. (2017); Fricke et al. (2017)). Narrower line widths can be achieved by even higher deuteration levels, where the exchangeable sites are back-protonated to only 10-50% in an otherwise fully deuterated environment (Chevelkov et al. (2006); Schanda et al. (2009); Linser et al. (2011b); Reif (2012)). Deuterated samples and 40-60 kHz MAS have enabled well-resolved proton-detected ssNMR experiments for structure determination (Huber et al. (2011); Knight et al. (2012); Zhou et al. (2007b); Linser et al. (2011a)) and detailed measurements of dynamics (Chevelkov et al. (2009); Tollinger et al. (2012); Schanda et al. (2011); Krushelnitsky et al. (2010); Smith et al. (2016)). However, the need for extensive deuteration is often a severe bottleneck, particularly when dealing with complex samples such as entire cell walls from bacteria that are difficult to culture in H_2O-based buffer and may be impossible to grow in D_2O media, or for proteins that are difficult to produce with deuterium labeling. Furthermore, the use of deuterated samples naturally eliminates the possibility of observing ^{1}H-^{13}C and ^{1}H-^{15}N correlation spectra, and thereby limits significantly the information content of the spectra.

Several recent applications have shown the resolution gains of even faster, sometimes termed "ultra-fast", MAS, *i.e.*, at spinning frequencies exceeding > 100 kHz. This technology is based on sample rotors of only 0.7 mm diameter, containing less than 1 μL, *i.e.*, only ca. 0.5 mg of sample. Although deuteration at these spinning frequencies is still beneficial to reduce line widths (Agarwal et al. (2014); Xue et al. (2017)), even fully protonated proteins yield relatively narrow ^{1}H line widths at > 100 kHz MAS of the order of 100-150 Hz (Stanek et al. (2016); Andreas et al. (2016); Xue et al. (2017)).

In this manuscript we show that well-resolved ^{1}H-detected correlation spectra of the intact peptidoglycan from bacterial cell wall of *Bacillus subtilis* can be obtained in a short experimental time using sub-milligram amounts at 100 kHz MAS frequencies. We present approaches for through-bond correlation experiments, required for assignment, and through-space ^{1}H-^{1}H correlation experiments, and explore the possibilities of studying peptidoglycan only with ^{1}H-^{1}H correlation experiments, thus removing the need for isotope labeling and opening new avenues to studies of cell walls of bacterial strains that are difficult to culture. In addition to the fact that the required sample amount is about an order of magnitude lower than for previously used ^{13}C-detected experiments, the availability of the additional ^{1}H frequency, alleviates problems due to overlap of ^{13}C frequencies and offers the possibility to follow cross-linking through amide resonances.

Materials and Methods

Sample preparation. Bacterial peptidoglycan sacculi have been prepared using methods described previously (Severin and Tomasz (1996); Kern et al. (2010)). Briefly, *Bacillus subtilis* subsp. *subtilis* strain 168 cells from the American Collection (ATCC 23857) were grown in standard M9 growth medium with ^{13}C glucose and ^{15}N ammonium chloride as sole carbon and nitrogen sources, respectively, or without isotope labeling. At an OD (600 nm) of ca. 0.7, cells were harvested by centrifugation at 5,500 g for 10 min and non covalently bound cell

wall components were removed by boiling in 4% w/v SDS for 30 min. The cell suspension was pelleted by ultracentrifugation at 25°C for 45 min at 130,000 g. The pellet was washed twice with 30 mL of 1 M NaCl and repeatedly with milli-Q water until it was free of SDS. The pellet was resuspended in 2 to 4 mL of deionized water, 1/3 volume of acid-washed glass beads (diameter of 0.17 to 0.18 mm) was added, and cells were disrupted. The glass beads were then separated from the cell lysate and the filtrate was centrifuged at 1,000 g for 5 min, and the supernatant, which contains the disrupted cell wall, was centrifuged at 130,000 g for 45 min at 25°C. The pellet was resuspended in 20 mL of 100 mM TrisHCl (pH 7.5) containing 20 mM $MgSO_4$. DNase A and RNase I were added to final concentrations of 10 and 50 µg/mL, respectively, and the sample was stirred for 2 h at 37°C. $CaCl_2$ (10 mM) and trypsin (100 µg/ml) were added, and the sample was stirred for 18 h at 37°C. Then, 1% SDS (final concentration) was added, and the sample was incubated for 15 min at 80°C to inactivate the enzymes. The cell wall was recovered by centrifugation for 45 min at 130,000 g at 25°C, resuspended with 20 mL of 8 M LiCl, and incubated for 15 min at 37°C. After another centrifugation, the pellet was resuspended in 10 mM ethylenediaminetetraacetic acid (EDTA) at pH 7.0 and incubated at 37°C for 15 min. The cell wall was washed with deionized water, acetone, and again with water before finally being resuspended in 2 to 4 mL of deionized water, yielding typically 50 mg of cell wall material for 1 L of culture. 5 mg of cell wall was then stirred with 48% hydrofluoric acid (HF) for 48 h at 4°C. The peptidoglycan was recovered by centrifugation at 130,000 g for 45 min at 4°C and washed with ice-cold deionized water, 100 mM TrisHCl (pH 7.0), and then twice with water and stirred at 4°C. This treatment resulted in intact well-hydrated peptidoglycan sacculi, which were resuspended in 50 mM HEPES buffer (pH 7.2) and filled into a Bruker 0.7 mm rotor using an ultracentrifuge spinning at 55,000 g during ca. 3 hours. To this end, the 0.7 mm rotor was inserted into a 1.3 mm rotor, which was inserted into a device for rotor-filling in an ultracentrifuge (Bruker Biospin).

NMR spectroscopy and data analysis. All experiments were performed on a Bruker Avance 2 spectrometer operating at a ^{1}H Larmor frequency of 950 MHz. The MAS frequency was set to 100 kHz and stable to within 5 Hz. Sample cooling was achieved with a cooling gas flow (300 L/h) at 273 K, while bearing and drive gas was at ca. 293 K. The resulting sample temperature under these conditions was determined with an external protein sample with the same MAS and temperature setup, using the bulk water resonance frequency and an internal DSS signal. The estimated sample temperature used in this study was ca. 30-32°C. Pulse sequences used in this study are shown in Figure 1. Typical 90°pulse durations were 2.1 µs (^{1}H, at 9 W), 2.7 µs (^{13}C, at 30 W) and 3.8 µs (^{15}N, at 30 W). Cross-polarization (CP) ^{1}H-^{15}N transfer was achieved with a 1 ms long ramped radiofrequency (RF) field strength of 60 to 80 kHz on ^{1}H and 30 kHz on ^{15}N. ^{1}H-^{13}C CP steps involved a ramped RF field on ^{1}H (115 to 140 kHz amplitude) and ca. 30 kHz RF field on ^{13}C, for 300 µs. Low-power WALTZ-16 (Shaka et al. (1983b)) decoupling was applied with RF field amplitudes of 10 kHz (^{1}H), 15 kHz (^{13}C) and 5 kHz (^{15}N). In INEPT-based transfers, the total transfer delay was 3.3 ms (^{1}H-^{13}C) and 4.4 ms (^{1}H-^{15}N). Solvent suppression follows the philosophy of the previously proposed MISSISSIPPI scheme (Zhou and Rienstra (2008)), *i.e.*, irradiation on ^{1}H while heteronuclear magnetization is stored along the z-axis, except that the irradiation scheme involved a train of back-to-back pulses with durations of 0.3 to 2 ms and 20 different phase settings. The aim of this essentially arbitrary pulse train is to create a 'random' phase trajectory. We find that this sequence offers superior solvent suppression than the original MISSISSIPPI scheme or with TPPM-based suppression schemes. The total duration of the solvent suppression was optimized and typically 30-60 ms. Radio-frequency driven ^{1}H-^{1}H recoupling (RFDR, Bennett et al. (1995)) elements were applied for 1.5 ms. TOCSY-type scalar-based ^{13}C-^{13}C transfer, according to the pulse scheme of Figure 1E, was achieved with the DIPSI scheme (Shaka et al. (1988)) at a ^{13}C RF field strength of 25 kHz. Two experiments were recorded with either 8 DISPI2 cycles (9.2 ms) or 12 cycles (13.8 ms). Spectra were processed with Topspin 3.5 (Bruker Biospin) and analyzed with

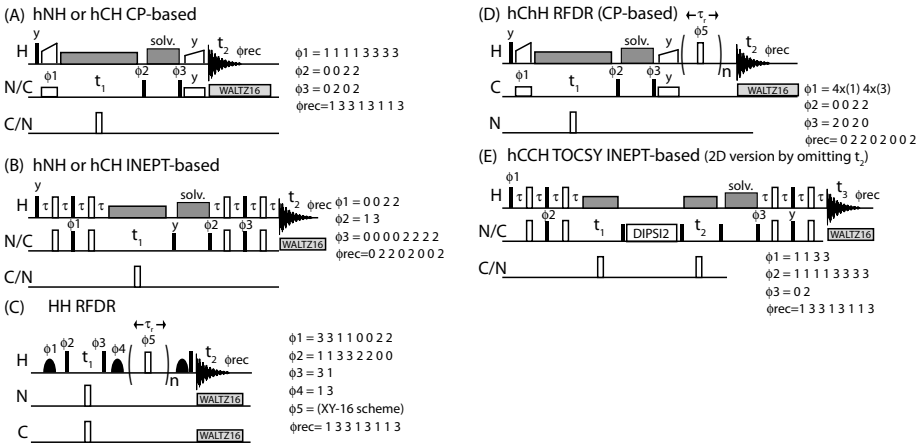

Figure 1: Pulse sequences used in this study for recording ^{1}H-^{15}N (A,B), ^{1}H-^{13}C (A,B,D,E) and ^{1}H-^{1}H (E) correlation spectra. Black rectangles and narrow open rectangles correspond to hard 90°and 180°pulses, respectively, and were applied at RF field strengths of 117 kHz (^{1}H), 90 kHz (^{13}C) and 65 kHz (^{15}N). Ramped cross-polarization (CP) is depicted with wide open symbols. ^{1}H decoupling was applied during the heteronuclear chemical-shift evolution periods with the WALTZ-16 (Shaka et al. (1983a)) scheme.

CcpNmr (Vranken et al. (2005)). ^{1}H chemical shifts were referenced according to the position of the resolved methyl group of the *N*-acetyl resonance of the *N*-acetylglucosamine (GlcNAc) moiety by comparison with the corresponding resonance in the liquid state. ^{13}C and ^{15}N chemical shifts were referenced indirectly using gyromagnetic ratios from the Biological Magnetic Resonance Data Bank.

Results and Discussion

A schematic chemical structure of the bacterial peptidoglycan is shown in Figure 2A. While the intact peptidoglycan has a total molecular weight of the order of gigadaltons, the constituting blocks are relatively limited, comprising a glycan backbone and peptide stems (in color), which may be cross-linked to the peptide stem of another glycan strand (in black). The two-dimensional spectra in red in Figure 2B-D show one-bond ^{1}H-^{15}N and ^{1}H-^{13}C correlations in intact peptidoglycan. Panel (B) reveals backbone and side-chain amide resonances from the peptide stems in addition to the *N*-acetyl resonances of the amino sugars. Panel (C) focuses on the ^{1}H-^{13}C region of the disaccharide motif resonances, while panel (D) shows the corresponding peptide portion of the spectrum. Additionally, a comparison of the CP-based to INEPT-based correlation spectra is shown in Supplementary Figure S1. The relative peak intensities in CP- *vs* INEPT-based experiments depend on the type of sub-motif studied. Resonances from the glycan strands, which correspond to more rigid portions than the peptide stems (Gansmueller et al. (2013)), are detected with more sensitivity in CP-based experiments, while peptide resonances are favored in the refocused-INEPT based experiments. Despite the very small amount of sample, these 2D ^{1}H-^{13}C correlation maps could be obtained in an experimental time of ca. 3 hours while the ^{1}H-^{15}N spectrum of Figure 2B was collected in 18 hours.

The ^{1}H line widths are in the order of 60-100 Hz for the ^{1}H-^{15}N sites, ca. 120 Hz for the carbohydrate ^{1}H-^{13}C sites and 50-150 Hz for the peptide ^{1}H-^{13}C sites (Figure 2), which allows resolving the majority of the sites. If the ability of the additional ^{1}H frequency to differentiate between different sites is not striking for the carbohydrate C1-C6 moieties due to severe overlaps of ^{1}H resonances on the contrary to ^{13}C frequencies (Figure 2C), its potential in raising the degeneracy of the 2,6-diaminopimelic acid (DAP) backbone (HN or HC at α position) *vs* side-chain (HN or HC at ϵ position) resonances or in raising the degeneracy of *N*-acetylglucosamine (GlcNAc) *vs* *N*-acetylmuramic acid (MurNAc) carbohydrates *N*-acetyl groups is clearly illustrated in Figure

2 parts B and D. The corresponding resonances are highly difficult to resolve in ^{13}C-^{13}C correlation maps as highlighted by the red rectangles in Figure S2. The increased resolution brought by the ^{1}H frequency is particularly noteworthy when it comes to follow the maturation of the peptidoglycan network through the degree of cross-linking at the DAP ϵ site (see DAP with 3-4 subscript labels in panels B and D of Figure 2 and see Table S6).

To assign the ^{1}H-^{13}C correlation spectra, we have recorded through-bond correlation spectra. Figure 1E shows the employed pulse sequence, which uses TOCSY mixing for efficient ^{13}C -^{13}C coherence transfer, and the resulting spectra are shown in Figure 2C,D and Supplementary Figure S1. Similarly to the case of proteins (Andreas et al. (2016)), the ^{13}C-^{13}C mixing scheme provides efficient transfer across multiple bonds, within experimental times of only ca. 1.5 days, despite the small amount of sample. These spectra proved particularly instrumental in the specific assignment of amidated *vs* non-amidated DAP (Dajkovic et al. (2017)), of crosslinked *vs* non-cross-linked DAP, and of L-Ala *vs* D-Ala (see Figure S3 for details).

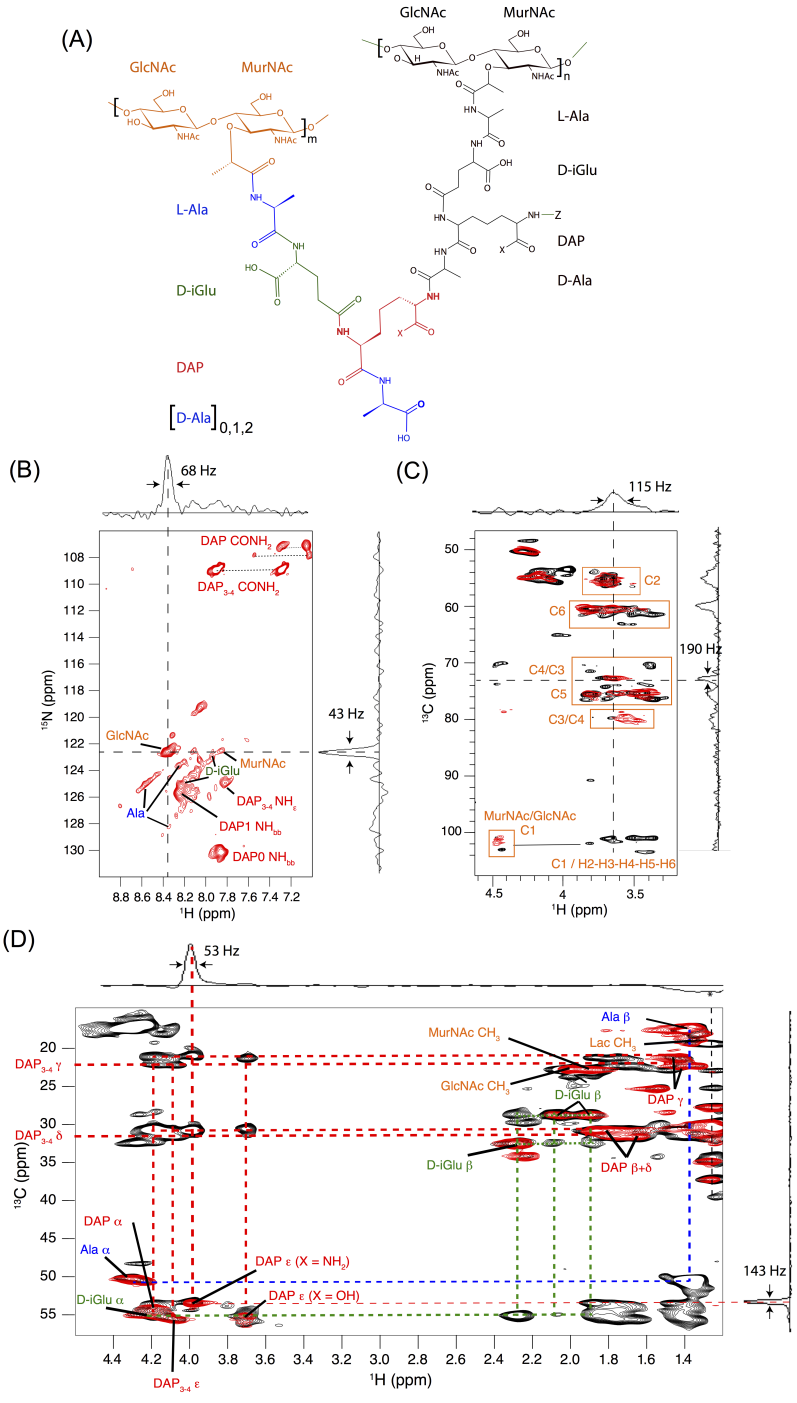
(A)
GlcNAc
MurNAc
L-Ala
D-iGlu
DAP
D-Ala
[D-Ala]0,1,2
(B)
68 Hz
DAP CONH2
DAP3-4 CONH2
GlcNAc
MurNAc
D-iGlu
Ala
DAP3-4 NHε
DAP1 NHbb
DAP0 NHbb
43 Hz
15N (ppm)
1H (ppm)
(C)
115 Hz
C2
C6
C4/C3
C5
C3/C4
190 Hz
MurNAc/GlcNAc C1
C1 / H2-H3-H4-H5-H6
13C (ppm)
1H (ppm)
(D)
53 Hz
MurNAc CH3
Ala β
Lac CH3
GlcNAc CH3
D-iGlu β
DAP γ
DAP3-4 γ
DAP3-4 δ
DAP β+δ
DAP α
Ala α
DAP ε (X = NH2)
D-iGlu α
DAP ε (X = OH)
DAP3-4 ε
143 Hz
13C (ppm)
1H (ppm)

Figure 2: Proton-detected solid-state NMR spectra of intact *Bacillus subtilis* peptidoglycan at 100 kHz for resonance assignment with through-bond experiments. (A) Chemical structure of peptidoglycan from *Bacillus subtilis*. Shown are two representative disaccharide units (top) from two different glycan strands of length m (in color) and n (in black), respectively. Each MurNAc of the glycan strand is connected to a peptide stem, which length and cross-linking vary during cell wall biosynthesis and maturation. Upon cross-linking, the D-Ala in position 4 of the donor stem (in black) binds to the amino group of DAP side-chain of the acceptor peptide stem (in color). This acceptor stem can contain 0, 1 or 2 C-terminal D-Ala as specified by the brackets. DAP0, DAP1, and DAP2 stand for DAP residues of corresponding acceptor stem tri-, tetra- and penta-peptide, respectively. The DAP side-chain of the donor stem (in black) can be either free (Z = H) or cross-linked (Z = another donor peptide stem). DAP in all stem peptides can be amidated (X = NH_2) or not (X = OH). DAP$3-4$ stand for a DAP residue of an acceptor stem cross-linked to the D-Ala of a donor stem. GlcNAc: *N*-acetylglucosamine (GlcNAc); MurNAc: *N*-acetylmuramic acid; DAP: 2,6-diaminopimelic acid; D-iGlu: D-*iso*glutamic acid. (B) ^{1}H-^{15}N correlation spectrum, based on INEPT transfer focusing on the amide region. (C) CP-based ^{1}H-^{13}C correlation spectrum focusing on the glycan region is shown in red. A two-dimensional hCcH TOCSY spectrum (omitting the second ^{13}C dimension in the pulse scheme of Figure 1E) is shown in black. (D) Amino acid aliphatic region of the ^{1}H-^{13}C correlation spectrum (red), and the 2D hCcH-TOCSY correlation map, showing through-bond correlations with dashed lines. The full peptide stem aliphatic and glycan parts of the spectra, with CP and INEPT-based transfer are shown in Figure S1. Different chemical moieties are labeled with different colors, corresponding to the color code in (A). 1D traces in Panels B-D are slices of the corresponding 2D spectra at the position of the black dotted lines with linewidth of the corresponding lines specified in Hz.

The ^{1}H-^{15}N correlation spectrum of intact peptidoglycan has lower intrinsic sensitivity than its ^{1}H-^{13}C counterpart, rendering triple-resonance experiments for assignments difficult. We tentatively ascribe this observation to chemical exchange of amide hydrogens with the solvent, as expected for flexible peptides at pH 7.5. We, thus, turned to solution-state spectra of peptidoglycan fragments, prepared by enzymatic digestion, to obtain site-specific assignments, which we further confirmed by homonuclear RFDR experiments (see below). Supplementary Figure S4 shows solution-state correlation spectra and experiments enabling the assignment of the ^{1}H-^{15}N spectrum. Briefly, the assignment followed well-established solution-state NMR techniques, involving HNCACB, hCCH-TOCSY and hCcoNH experiments. Figure 2B reports the assignments on the 100 kHz MAS spectrum for those peaks that show similar cross-peak positions in solution and solid-state samples. Interestingly, while showing several similarities, the spectrum of the intact peptidoglycan sacculi differs in peak intensities and peak positions significantly from the fragments. This observation demonstrates that the structure and dynamics of intact PG differs from those of fragments, illustrating the importance of studying intact samples rather than fragments for gaining insight into the native peptidoglycan properties.

Lastly, we have explored the possibilities of obtaining dipolar (*i.e.*, through-space) proximities through ^{1}H-^{1}H dipolar recoupling experiments with the RFDR scheme (Figure 1C,D). Figure 3A shows a two-dimensional ^{1}H-^{1}H correlation experiment, and Figure 3B shows a two-dimensional ^{13}C-edited experiment which encodes ^{1}H-^{1}H contacts, based on the pulse scheme shown in Figure 1D. The latter experiment is particularly useful for the glycan sites, which have ^{1}H resonance frequencies close to the one of bulk water, such that the residual solvent signal in the homonuclear experiment makes extraction of these signals difficult (Figure S5B).

In these two experiments numerous contacts between protons in spatial proximity are visible. While the majority of the contacts are within the same amino acid or within the same sugar, inter-residue contacts in the amide region of the spectrum in Figure 3A between the DAP amide resonances and D-iGlu

Hβ and Hγ yield unambiguous identification of the DAP residues. In the ^{13}C-edited spectrum in Figure 3B a series of spectrally unambiguous remarkable cross-peaks are the ones connecting the HN, H2 and N-acetyl methyl sites of the GlcNAc sugar moiety with the H$^{\alpha}$ of the neighboring L-alanine residue on the MurNAc peptide stem. While currently there are no atomic structures of peptidoglycan available, the distance between these nuclei exceeds at least ca. 5 Å.

Conclusions

Recent ssNMR investigations on protein samples (Andreas et al. (2016); Agarwal et al. (2014)), established that high-resolution spectra and even atomic-resolution protein structures can be obtained at $>$ 100 kHz MAS. We have shown here that intact bacterial peptidoglycan sacculi yield highly resolved ^{1}H-detected correlation spectra. Despite the very small amount of sample required (0.5 mg), it is possible to obtain site-specific resonance assignments and information about spatial proximities. The sensitivity of these experiments shall also allow the study of the dynamics of intact cell walls. Indeed, high MAS frequencies suppress artifacts in dynamics measurements, and render quantitative analyses possible (Lewandowski et al. (2011b); Schanda and Ernst (2016)), such that the ultra-fast MAS is doubly favorable, providing high-resolution spectra and facilitating quantitative measurements.

We foresee that ultra-fast MAS NMR experiments will also be instrumental for determining the structures of proteins bound to peptidoglycan. A recent study has determined the binding pose of a protein bound to the cell wall at ca. 40 kHz MAS (Schanda et al. (2014)), but provided information primarily for the protein rather than for peptidoglycan. The high sensitivity and resolution with which the peptidoglycan can be observed at ultra-fast MAS may allow NMR experiments to provide a more comprehensive picture of such complexes.

The availability of ^{1}H-detected spectra may also provide useful information about the structure of peptidoglycan. While the ^{1}H-^{1}H distances obtained here

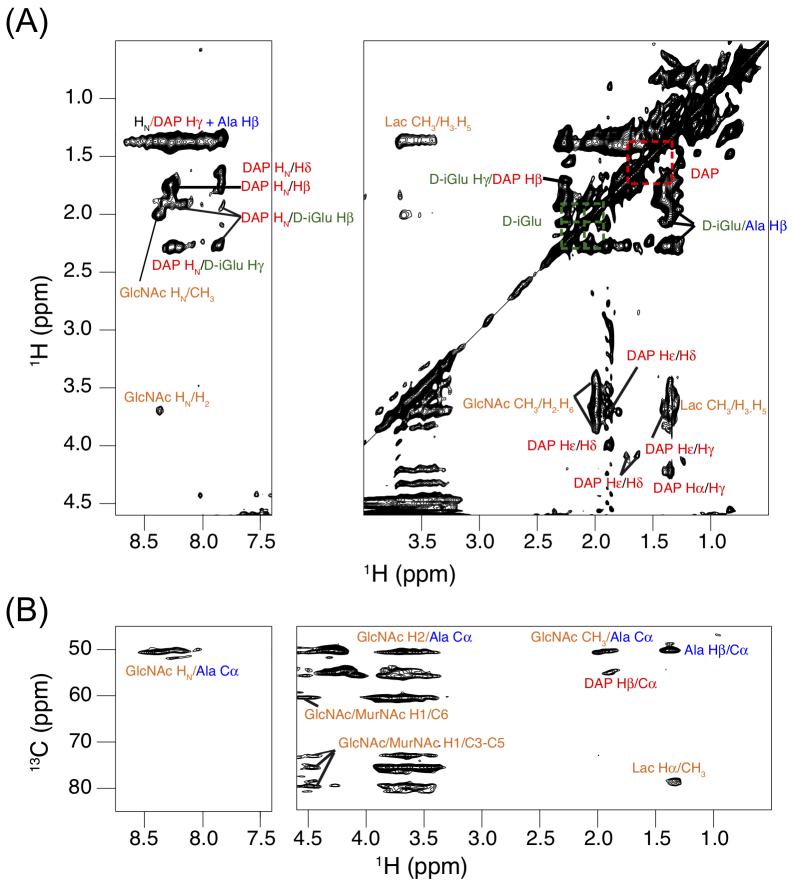

Figure 3: Dipolar ^{1}H-^{1}H correlation spectra using radio-frequency driven recoupling (RFDR) of the ^{1}H-^{1}H interaction. (A) Homonuclear 2D correlation experiment and (B) ^{13}C-edited ^{1}H-^{1}H correlation, focusing on the glycan part. The full-width spectrum is shown in Supplementary Figure S5. Both experiments have been collected with a 1.5 ms RFDR mixing at a MAS frequency of 100 kHz. Assignments of the correlation peaks are indicated and color-coded according to the color scheme shown in Figure 2A. Note that solvent suppression is a significant challenge in this experiment. We have used a flip-back pulse to alleviate this problem (see Figure 1). Its application results in a ca. 3-4 fold reduction of the solvent signal, but the residual solvent signal remains a dominant contribution. Exchanging the buffer to D_2O is a viable solution, but it comes at the cost of losing all exchange-labile hydrogens; as the amide proton signals contain important information, we present in this study only data from H_2O based samples.

with RFDR experiments are rather short-range, and thus not likely to provide much structural information, the ease and sensitivity of these experiments shall enable longer-range distance measurements. For example, the attachment of spin labels to specific sites on the peptidoglycan or to interacting proteins may provide rapid and quantitative distance estimates from paramagnetic relaxation enhancement, possibly contributing to refining the view of the structural organization of this important biopolymer.

This exploratory study also shows that it is possible to obtain "fingerprint" homonuclear ^{1}H-^{1}H correlation spectra, *i.e.*, to study complex biological systems without isotope labeling, which opens new fields of applications to NMR spectroscopy in which so far it has been difficult to obtain any atomic-resolution information.

Acknowledgements

This work used the platforms of the Grenoble Instruct Center (ISBG; UMS 3518 CNRS-CEA- UJF-EMBL) with support from FRISBI (ANR-10-INSB-05-02) and GRAL (ANR-10-LABX-49-01) within the Grenoble Partnership for Structural Biology (PSB). P.S. acknowledges support from the European Research Council (ERC-Stg- 311318) and C.B. and J.-P.S. aknowledge support from the ANR grant ANR-16-CE11-0030-01.

References

Agarwal V, Penzel S, Szekely K, Cadalbert R, Testori E, Oss A, Past J, Samoson A, Ernst M, Böckmann A, Meier BH. De novo 3D structure determination from sub-milligram protein samples by solid-state 100 kHz MAS NMR spectroscopy. Angew Chem Int Ed Engl 2014;53(45):12253–6. doi:10.1002/anie.201405730.

Andreas LB, Jaudzems K, Stanek J, Lalli D, Bertarello A, Le Marchand T, Cala-De Paepe D, Kotelovica S, Akopjana I, Knott B, Wegner S, Engelke F,

Lesage A, Emsley L, Tars K, Herrmann T, Pintacuda G. Structure of fully protonated proteins by proton-detected magic-angle spinning NMR. Proc Natl Acad Sci 2016;113(33):9187–92. doi:10.1073/pnas.1602248113.

Bennett AE, Rienstra CM, Auger M, Lakshmi KV, Griffin RG. Heteronuclear Decoupling in Rotating Solids. J Chem Phys 1995;103(16):6951–8.

Bertini I, Bhaumik A, De Paëpe G, Griffin RG, Lelli M, Lewandowski JR, Luchinat C. High-resolution solid-state NMR structure of a 17.6 kDa protein. J Am Chem Soc 2010;132(3):1032–40. doi:10.1021/ja906426p.

Castellani F, van Rossum B, Diehl A, Schubert M, Rehbein K, Oschkinat H. Structure of a protein determined by solid-state magic-angle-spinning NMR spectroscopy. Nature 2002;420(6911):98–102. doi:10.1038/nature01070.

Cegelski L, Kim SJ, Hing AW, Studelska DR, O'Connor RD, Mehta AK, Schaefer J. Rotational-echo double resonance characterization of the effects of vancomycin on cell wall synthesis in *Staphylococcus aureus*. Biochemistry 2002;41(43):13053–8.

Cegelski L, OConnor RD, Stueber D, Singh M, Poliks B, Schaefer J. Plant cell-wall cross-links by redor nmr spectroscopy. J Am Chem Soc 2010;132(45):16052–7.

Chevelkov V, Fink U, Reif B. Quantitative analysis of backbone motion in proteins using MAS solid-state NMR spectroscopy. J Biomol NMR 2009;45(1-2):197–206. doi:10.1007/s10858-009-9348-5.

Chevelkov V, Rehbein K, Diehl A, Reif B. Ultrahigh resolution in proton solid-state NMR spectroscopy at high levels of deuteration. Angew Chem Int Ed Engl 2006;45(23):3878–81. doi:10.1002/anie.200600328.

Comellas G, Rienstra CM. Protein structure determination by magic-angle spinning solid-state NMR, and insights into the formation, structure, and stability of amyloid fibrils. Annu Rev Biophys 2013;42:515–36.

Dajkovic A, Tesson B, Chauhan S, Courtin P, Keary R, Flores P, Marlière C, Filipe SR, Chapot-Chartier MP, Carballido-Lopez R. Hydrolysis of peptidoglycan is modulated by amidation of meso-diaminopimelic acid and mg2+ in bacillus subtilis. Mol Microbiol 2017;104(6):972–88.

Delaglio F, Grzesiek S, Vuister G, Zhu G, Pfeifer J, Bax A. NMRPIPE - a multidimensional spectral processing system based on Unix pipes. J Biomol NMR 1995;6(3):277–93.

Dick-Perez M, Zhang Y, Hayes J, Salazar A, Zabotina OA, Hong M. Structure and interactions of plant cell-wall polysaccharides by two- and three-dimensional magic-angle-spinning solid-state NMR. Biochemistry 2011;50(6):989–1000.

Fraga H, Arnaud CA, Gauto DF, Audin M, Kurauskas V, Macek P, Krichel C, Guan JY, Boisbouvier J, Sprangers R, Breyton C, Schanda P. Solid-State NMR H-N-(C)-H and H-N-C-C 3D/4D Correlation Experiments for Resonance Assignment of Large Proteins. ChemPhysChem 2017;18(19):2697–703. URL: http://doi.wiley.com/10.1002/cphc.201700572. doi:10.1002/cphc.201700572.

Fricke P, Chevelkov V, Zinke M, Giller K, Becker S, Lange A. Backbone assignment of perdeuterated proteins by solid-state NMR using proton detection and ultrafast magic-angle spinning. Nat Protoc 2017;12(4):764–82. doi:10.1038/nprot.2016.190.

Gansmueller A, Simorre JP, Hediger S. Windowed R-PDLF recoupling: A flexible and reliable tool to characterize molecular dynamics. Journal of Magnetic Resonance 2013;234:154–64. doi:10.1016/j.jmr.2013.06.017.

Glauner B. Separation and quantification of muropeptides with high-performance liquid chromatography. Analytical biochemistry 1988;172(2):451–64.

Grzesiek S, Bax A. Amino acid type determination in the sequential assignment procedure of uniformly 13 c/15 n-enriched proteins. J Biomol NMR 1993;3(2):185–204.

Hu W, Kakalis LT, Jiang L, Jiang F, Ye X, Majumdar A. 3d hcch-cosy-tocsy experiment for the assignment of ribose and amino acid side chains in 13c labeled rna and protein. J Biomol NMR 1998;12(4):559–64.

Huber M, Hiller S, Schanda P, Ernst M, Böckmann A, Verel R, Meier BH. A proton-detected 4D solid-state NMR experiment for protein structure determination. ChemPhysChem 2011;12(5):915–8.

Kern T, Giffard M, Hediger S, Amoroso A, Giustini C, Bui NK, Joris B, Bougault C, Vollmer W, Simorre JP. Dynamics characterization of fully hydrated bacterial cell walls by solid-state NMR: evidence for cooperative binding of metal ions. Journal of the American Chemical Society 2010;132(31):10911–9. doi:10.1021/ja104533w.

Kern T, Hediger S, Müller P, Giustini C, Joris B, Bougault C, Vollmer W, Simorre JP. Toward the characterization of peptidoglycan structure and protein-peptidoglycan interactions by solid-state NMR spectroscopy. J Am Chem Soc 2008;130:5618–9. doi:10.1021/ja7108135.

Kim SJ, Cegelski L, Preobrazhenskaya M, Schaefer J. Structures of *Staphylococcus aureus* cell-wall complexes with vancomycin, eremomycin, and chloroeremomycin derivatives by 13c {19F} and 15n {19F} rotational-echo double resonance. Biochemistry 2006;45(16):5235–50.

Kim SJ, Matsuoka S, Patti GJ, Schaefer J. Vancomycin Derivative with Damaged D -Ala- D -Ala Binding Cleft Binds to Cross-linked Peptidoglycan in the Cell Wall of Staphylococcus aureus . Biochemistry 2008;(47):3822–31.

Knight MJ, Pell AJ, Bertini I, Felli IC, Gonnelli L, Pierattelli R, Herrmann T, Emsley L, Pintacuda G. Structure and backbone dynamics of a mi-

crocrystalline metalloprotein by solid-state nmr. Proc Natl Acad Sci USA 2012;109(28):11095–100.

Krushelnitsky A, Zinkevich T, Reichert D, Chevelkov V, Reif B. Microsecond time scale mobility in a solid protein as studied by the 15N R(1rho) site-specific NMR relaxation rates. J Am Chem Soc 2010;132(34):11850–3. doi:10.1021/ja103582n.

Lescop E, Kern T, Brutscher B. Guidelines for the use of band-selective radiofrequency pulses in hetero-nuclear NMR: Example of longitudinal-relaxation-enhanced BEST-type 1H15N correlation experiments. J Magn Reson 2010;203(1):190–8. doi:10.1016/j.jmr.2009.12.001.

Lescop E, Schanda P, Rasia R, Brutscher B. Automated spectral compression for fast multidimensional NMR and increased time resolution in real-time NMR spectroscopy. J Am Chem Soc 2007;129(10):2756–7. doi:10.1021/ja068949u.

Lewandowski JR, Dumez JN, Akbey U, Lange S, Emsley L, Oschkinat H. Enhanced Resolution and Coherence Lifetimes in the Solid-state NMR Spectroscopy of Perdeuterated Proteins under Ultrafast Magic-angle Spinning. J Phys Chem Lett 2011a;2(17):2205–11.

Lewandowski JR, Sass HJr, Grzesiek S, Blackledge M, Emsley L. Site-specific measurement of slow motions in proteins. J Am Chem Soc 2011b;133(42):16762–5.

Li K, Yuan XX, Sun HM, Zhao LS, Tang R, Chen ZH, Qin QL, Chen XL, Zhang YZ, Su HN. Atomic force microscopy of side wall and septa peptidoglycan from bacillus subtilis reveals an architectural remodeling during growth. Front Microbiol 2018;9:620.

Linser R, Bardiaux B, Higman V, Fink U, Reif B. Structure calculation from unambiguous long-range amide and methyl 1H-1H distance restraints for a microcrystalline protein with MAS solid-state NMR spectroscopy. J Am Chem Soc 2011a;133(15):5905–12.

Linser R, Dasari M, Hiller M, Higman V, Fink U, Lopez del Amo JM, Markovic S, Handel L, Kessler B, Schmieder P, Oesterhelt D, Oschkinat H, Reif B. Proton-detected solid-state NMR spectroscopy of fibrillar and membrane proteins. Angew Chem Int Ed Engl 2011b;50(19):4508–12.

Loquet A, Sgourakis NG, Gupta R, Giller K, Riedel D, Goosmann C, Griesinger C, Kolbe M, Baker D, Becker S, Lange A. Atomic model of the type III secretion system needle. Nature 2012;486(7402):276–9. doi:10.1038/nature11079. arXiv:NIHMS150003.

Marchetti A, Jehle S, Felletti M, Knight MJ, Wang Y, Xu Zq, Park AY, Otting G, Lesage A, Emsley L, Dixon NE, Pintacuda G. Backbone Assignment of Fully Protonated Solid Proteins by 1 H Detection and Ultrafast Magic-Angle-Spinning NMR Spectroscopy. Angew Chem Int Ed Engl 2012;51(43):10756–9. doi:10.1002/anie.201203124.

Morag O, Sgourakis NG, Baker D, Goldbourt A. The NMRRosetta capsid model of M13 bacteriophage reveals a quadrupled hydrophobic packing epitope. Proc Natl Acad Sci 2015;112(4):971–6. URL: http://www.pnas.org/lookup/doi/10.1073/pnas.1415393112. doi:10.1073/pnas.1415393112.

Park SH, Das BB, Casagrande F, Tian Y, Nothnagel HJ, Chu M, Kiefer H, Maier K, Angelis AAD, Marassi FM, Opella SJ. Structure of the chemokine receptor CXCR1 in phospholipid bilayers. Nature 2012;491:779–83. doi:10.1038/nature11580.

Pazos M, Peters K, Vollmer W. Robust peptidoglycan growth by dynamic and variable multi-protein complexes. Curr Opin Microbiol 2017;36:55–61.

Reif B. Ultra-high resolution in MAS solid-state NMR of perdeuterated proteins: Implications for structure and dynamics. J Magn Reson 2012;216:1–12. doi:10.1016/j.jmr.2011.12.017.

Renault M, Tommassen-van Boxtel R, Bos MP, Post JA, Tommassen J, Baldus

M. Cellular solid-state nuclear magnetic resonance spectroscopy. Proc Natl Acad Sci USA 2012;109(13):4863–8.

Renault M, Cukkemane A, Baldus M. Solid-state NMR spectroscopy on complex biomolecules. Angew Chem Int Ed Engl 2010;49(45):8346–57. doi:10.1002/anie.201002823.

Romaniuk JA, Cegelski L. Bacterial cell wall composition and the influence of antibiotics by cell-wall and whole-cell nmr. Phil Trans R Soc B 2015;370(1679):20150024.

Schanda P, Ernst M. Studying dynamics by magic-angle spinning solid-state NMR spectroscopy: Principles and applications to biomolecules. Prog Nucl Magn Reson Spectr 2016;96:1–46. doi:10.1016/j.pnmrs.2016.02.001. arXiv:arXiv:1011.1669v3.

Schanda P, Huber M, Boisbouvier J, Meier BH, Ernst M. Solid-state NMR measurements of asymmetric dipolar couplings provide insight into protein side-chain motion. Angew Chem Int Ed 2011;50(46):11005–9.

Schanda P, Huber M, Verel R, Ernst M, Meier BH. Direct Detection of 3hJNC' Hydrogen-Bond Scalar Couplings in Proteins by Solid-State NMR Spectroscopy. Angew Chem Int Ed Engl 2009;48(49):9322–5. doi:10.1002/anie.200904411.

Schanda P, Kupče , Brutscher B, Kupče E, Brutscher B. SOFAST-HMQC experiments for recording two-dimensional deteronuclear correlation spectra of proteins within a few seconds. J Biomol NMR 2005;33(4):199–211. doi:10.1007/s10858-005-4425-x.

Schanda P, Triboulet S, Laguri C, Bougault CM, Ayala I, Callon M, Arthur M, Simorre JP. Atomic model of a cell-wall cross-linking enzyme in complex with an intact bacterial peptidoglycan. Journal of the American Chemical Society 2014;136(51):17852–60. doi:10.1021/ja5105987.

Severin A, Tomasz A. Naturally occurring peptidoglycan variants of *Streptococcus pneumoniae*. J Bacteriol 1996;178(1):168–74.

Shahid SA, Bardiaux B, Franks WT, Krabben L, Habeck M, van Rossum BJ, Linke D. Membrane-protein structure determination by solid-state nmr spectroscopy of microcrystals. Nat Meth 2012;9(12):1212.

Shaka A, Lee C, Pines A. Iterative schemes for bilinear operators; application to spin decoupling. J Magn Reson 1988;77(2):274–93.

Shaka AJ, Keeler J, Freeman R. Evaluation of a new broad-band decoupling sequence - WALTZ-16. J Magn Reson 1983a;53(2):313–40.

Shaka AJ, Keeler J, Frenkiel T, Freeman R. An improved sequence for broad-band decoupling: WALTZ-16. J Magn Reson 1983b;52(2):335–8. doi:10.1016/0022-2364(83)90207-X.

Smith AA, Testori E, Cadalbert R, Meier BH, Ernst M. Characterization of fibril dynamics on three timescales by solid-state NMR. J Biomol NMR 2016;65(3-4):171–91. doi:10.1007/s10858-016-0047-8.

Stanek J, Andreas LB, Jaudzems K, Cala D, Lalli D, Bertarello A, Schubeis T, Akopjana I, Kotelovica S, Tars K, Pica A, Leone S, Picone D, Xu ZQ, Dixon NE, Martinez D, Berbon M, El Mammeri N, Noubhani A, Saupe S, Habenstein B, Loquet A, Pintacuda G. NMR Spectroscopic Assignment of Backbone and Side-Chain Protons in Fully Protonated Proteins: Microcrystals, Sedimented Assemblies, and Amyloid Fibrils. Angew Chem Int Ed 2016;55(50):15504–9. doi:10.1002/anie.201607084.

Sun ZYJ, Hyberts SG, Rovnyak D, Park S, Stern AS, Hoch JC, Wagner G. High-resolution aliphatic side-chain assignments in 3d hcconh experiments with joint h–c evolution and non-uniform sampling. J Biomol NMR 2005;32(1):55–60.

Tollinger M, Sivertsen AC, Meier BH, Ernst M, Schanda P. Site-resolved measurement of microsecond-to-millisecond conformational-exchange pro-

cesses in proteins by solid-state NMR spectroscopy. J Am Chem Soc 2012;134(36):14800–7. doi:10.1021/ja303591y.

Tong G, Pan Y, Dong H, Pryor R, Wilson GE, Schaefer J. Structure and dynamics of pentaglycyl bridges in the cell walls of *Staphylococcus aureus* by 13C- 15N REDOR NMR. Biochemistry 1997;36(32):9859–66.

Turner RD, Mesnage S, Hobbs JK, Foster SJ. Molecular imaging of glycan chains couples cell-wall polysaccharide architecture to bacterial cell morphology. Nat Commun 2018;9(1):1263.

Vranken WF, Boucher W, Stevens TJ, Fogh RH, Pajon A, Llinas M, Ulrich EL, Markley JL, Ionides J, Laue ED. The CCPN data model for NMR spectroscopy: Development of a software pipeline. Proteins-Structure Function and Bioinformatics 2005;59(4):687–96.

Wang S, Munro RA, Shi L, Kawamura I, Okitsu T, Wada A, Kim SY, Jung KH, Brown LS, Ladizhansky V. Solid-state NMR spectroscopy structure determination of a lipid-embedded heptahelical membrane protein. Nat Methods 2013a;10:1007–12. doi:10.1038/nmeth.2635.

Wang T, Park YB, Caporini MA, Rosay M, Zhong L, Cosgrove DJ, Hong M. Sensitivity-enhanced solid-state nmr detection of expansins target in plant cell walls. Proc Natl Acad Sci USA 2013b;110(41):16444–9.

Xue K, Sarkar R, Motz C, Asami S, Camargo DCR, Decker V, Wegner S, Tosner Z, Reif B. Limits of Resolution and Sensitivity of Proton Detected MAS Solid-State NMR Experiments at 111 kHz in Deuterated and Protonated Proteins. Sci Rep 2017;7(1):7444–50.

Zhou D, Rienstra C. High-performance solvent suppression for proton detected solid-state NMR. J Magn Reson 2008;192(1):167–72.

Zhou DH, Shah G, Cormos M, Mullen C, Sandoz D, Rienstra CM. Proton-detected solid-state NMR spectroscopy of fully protonated proteins at 40 kHz

magic-angle spinning. J Am Chem Soc 2007a;129(38):11791–801. doi:10.1021/ja073462m.

Zhou DH, Shea JJ, Nieuwkoop AJ, Franks WT, Wylie BJ, Mullen C, Sandoz D, Rienstra CM. Solid-State Protein-Structure Determination with Proton-Detected Triple-Resonance 3D Magic-Angle-Spinning NMR Spectroscopy. Angew Chemie 2007b;119(44):8532–5. doi:10.1002/ange.200702905.

Supporting Information

Preparation of *B. subtilis* fragments for solution-state NMR

^{13}C,^{15}N-labeled peptidoglycan soluble fragments were obtained by digestion of the intact uniformly-labeled peptidoglycan sacculi according to previously published procedure (Glauner (1988)). A peptidoglycan suspension (5 mg in 2 mL) was incubated with 100 μg of Cellosyl in 20 mM sodium phosphate buffer pH 4.8 for 24 hours at 37 °C. The reaction was stopped by Cellulosyl denaturation at 100 °C for 10 min and non-digested material as well as denatured enzyme were removed by centrifugation for 10 min at 13,000 g. The supernatant was extensively dialyzed against water using a membrane with 500 Da cutoff and the soluble uniformly-labeled peptidoglycan fragments were lyophilized for storage. A fresh NMR sample was prepared by solubilizing the peptidoglycan fragments in water containing 10% D_2O. pH was adjusted to 7.0 using diluted NaOH solution.

Solution-state NMR spectroscopy

Solution-state NMR spectra were acquired on Agilent 600- or 800-MHz spectrometers equipped with a triple resonance cryogenic probe. Data collection included ^{15}N-SOFAST (Schanda et al. (2005)), ^{13}C-CT-HSQC (Grzesiek and Bax (1993)), 3D-BEST-HNCACB and HNCO (Lescop et al. (2007)), 2D hCcH-TOCSY ((Hu et al. (1998)), and 2D hCconH (Sun et al. (2005)) experiments. Data were processed with NmrPipe (Delaglio et al. (1995)) and analyzed in CcpNmr (Vranken et al. (2005)). Amino acid ^1H, ^{13}C and ^{15}N-backbone resonances were assigned using a combination of 3D Best-HNCACB and 3D Best-HNCO experiments collected for a total duration of 11 and 1.5 hours, respectively. A 2D version of the HCCH-TOCSY experiment was used to identify amino acid side-chain and carbohydrate ^1H- and ^{13}C-resonances. Specific resonance assignment in the peptide stems was achieved using the hCconH experiment. The combined analysis of the 2D hCconH and 3D HNCACB experiments was particularly usefull in discriminating the DAP0 and DAP1/2 backbone amide resonances for

this residue involved in tri- or tetra-/penta-peptide stems, respectively, and the DAP side-chain amide resonance at position ϵ when this residue is involved in a cross-link with the D-Ala of a peptide donor stem (see Figure S4.

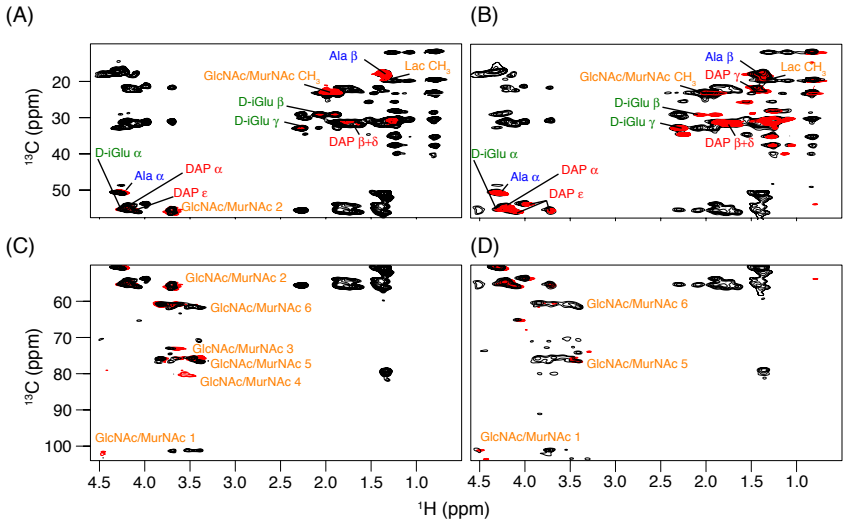

Figure S1: Comparison of cross-polarization based (A,C) and refocused-INEPT-based (B,D) ^{1}H-^{13}C correlation spectra of intact *B. subtilis* peptidoglycan, recorded with the pulse sequences shown in Figure 1A and 1B of the main text, respectively, at 100 kHz MAS frequency. The CP-based spectrum, in red in panels A and C, is superimposed with the INEPT-based hCcH-TOCSY experiment in black collected with a long 13.8-ms ^{13}C-^{13}C transfer, while the refocused-INEPT-based spectrum, in red in panels B and D, is overlaid with the INEPT-based hCcH-TOCSY experiment in black collected with a short 9.8-ms ^{13}C-^{13}C transfer. A comparison between panels A and B emphasizes the increased sensitivity of refocused-INEPT experiments to track peptide stem ^{1}H-^{13}C correlations, as the DAP-γ correlation is missing in panel A. A comparison between panels A and B emphasizes the increased sensitivity of CP-based experiments to track carbohydrate ^{1}H-^{13}C correlations, as most correlations at sugar positions 1 through 5 are absent in panel D.

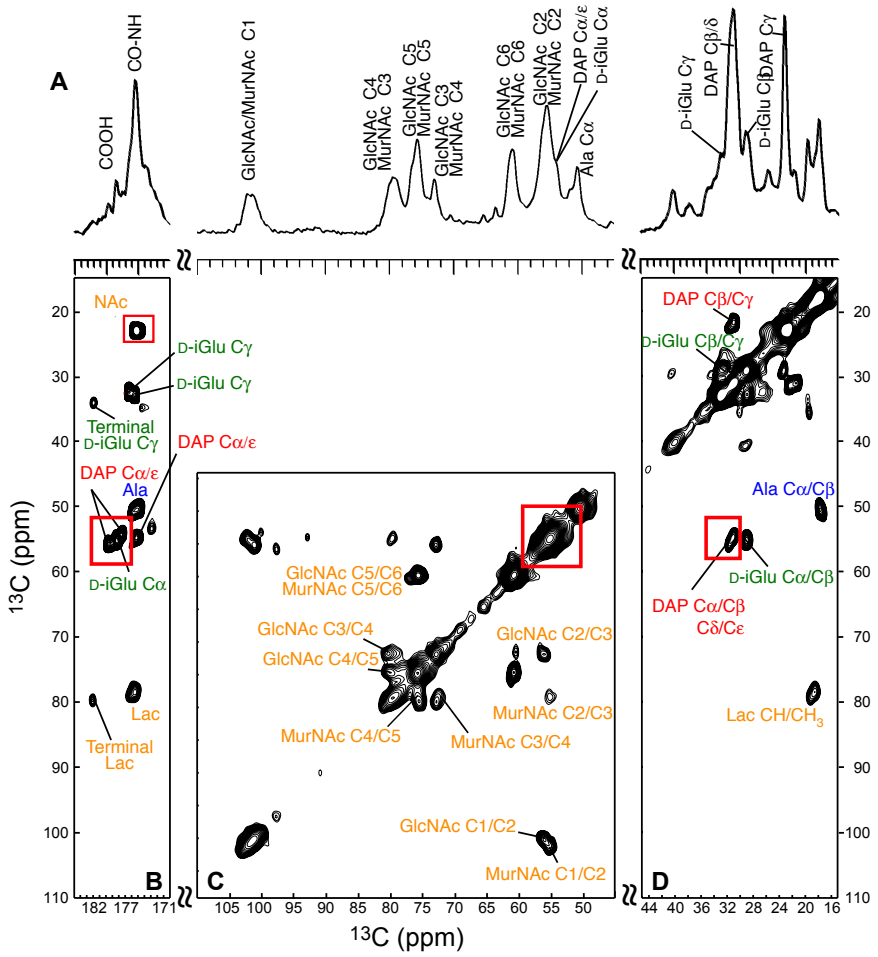

Figure S2: ^{13}C-detected solid-state NMR spectra of a fully ^{13}C,^{15}N-uniformly labeled intact peptidoglycan sample of *B. subtilis* experiment of peptidoglycan collected at 12.5 kHz MAS frequency, 9.4 T and 283 K. (A) 1D ^{13}C-CPMAS spectrum and (B-D) portions of the 2D through-bond ^{13}C-^{13}C correlation spectrum (see (Kern et al. (2008)) for the pulse sequence). (B) shows correlations between backbone or side-chain carbonyls and Cα or Cϵ, respectively, of individual amino acids, as well as of *N*-acetylglucosamine (GlcNAc) and *N*-acetylmuramic acid (MurNAc). (C) and (D) emphasize correlations between sugar carbons and amino acid side-chains, respectively. All residues are color-coded according to the peptidoglycan constituting motif detailed in Figure 2A of the main text. Red rectangles outline areas, where resolution of the ^{13}C resonances is lacking.

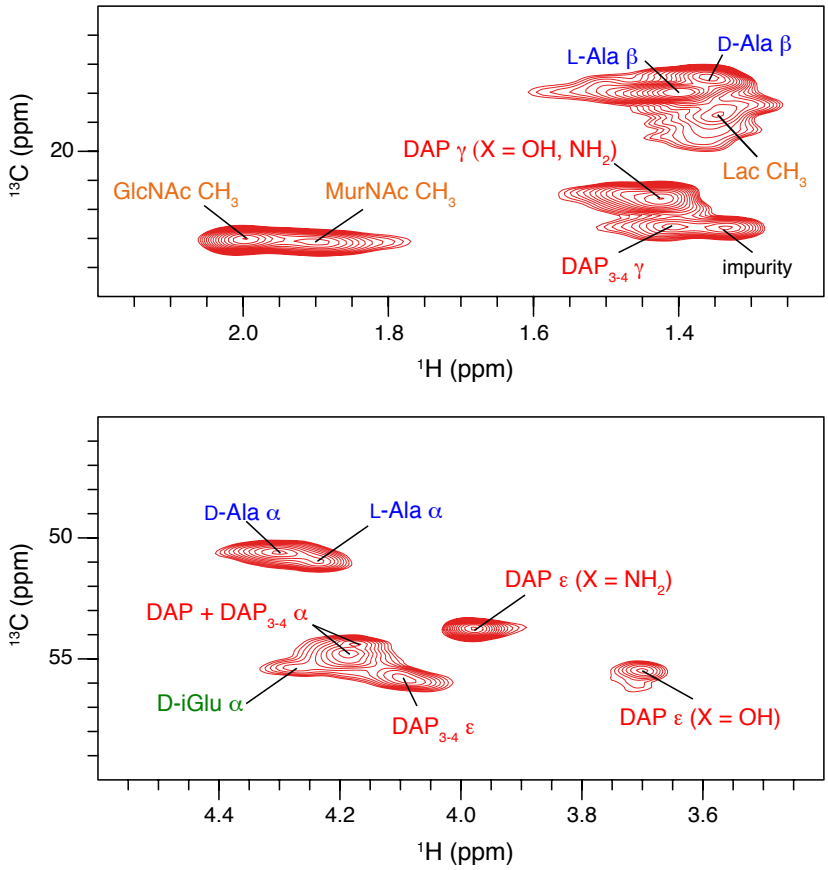

Figure S3: Excerpts of the INEPT-based ^{1}H-^{13}C- correlation spectrum detailing resolution and resonance assignments of the DAP (lower panel) at positions α and ϵ, and of L-Ala *vs* D-Ala at positions α and β (upper panel).

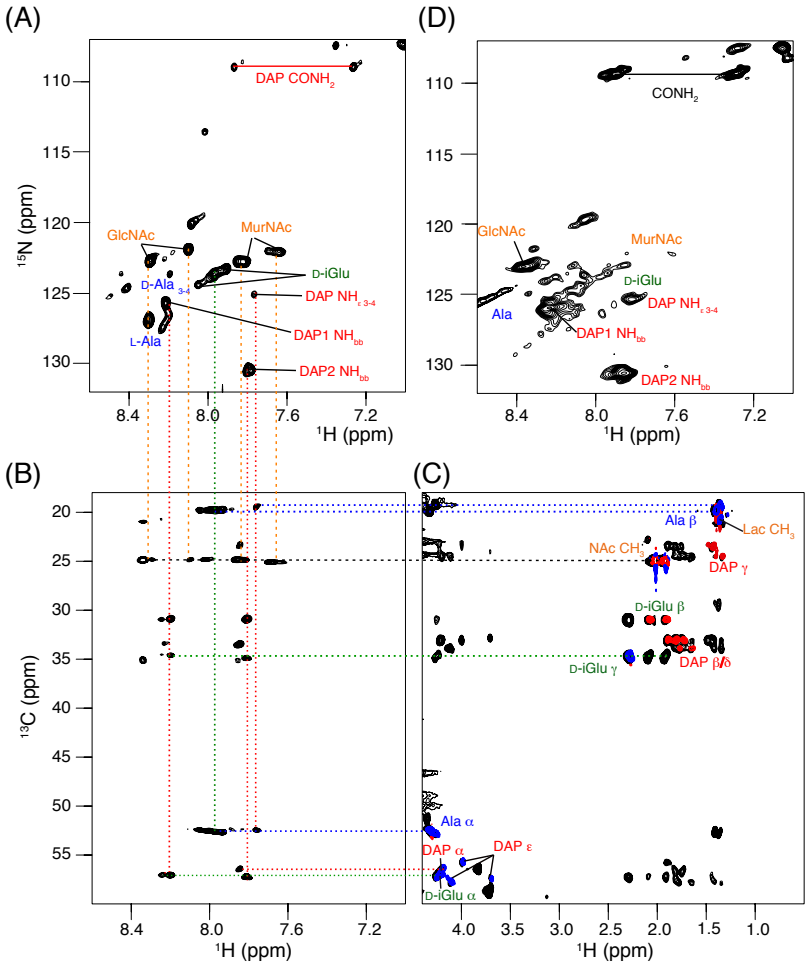
(A)
(D)
(B)
(C)
DAP CONH2
CONH2
GlcNAc
MurNAc
D-iGlu
D-Ala 3-4
DAP NH ε 3-4
L-Ala
Ala
DAP1 NHbb
DAP2 NHbb
15N (ppm)
1H (ppm)
13C (ppm)
Ala β
Lac CH3
NAc CH3
DAP γ
D-iGlu β
D-iGlu γ
DAP β/δ
Ala α
DAP α
DAP ε
D-iGlu α

Figure S4: (Preceding page) Comparison of ^{1}H-^{15}N correlation experiments recorded on soluble peptidoglycan fragments, obtained by enzymatic digestion, and on intact peptidoglycan. (A) ^{15}N-SOFAST-HSQC experiment collected on a few hundreds of µM of *B. subtilis* peptidoglycan fragments in H_2O at pH 7.0 and 37 °C. The spectrum was recorded in 20 min on a 600 MHz Agilent spectrometer equipped with a cryoprobe. Assignment of resonances in this spectrum is obtained from the 2D spectra presented in panels B and C, complemented with a 3D BEST-HNCACB collected for 11 hours according to the pulse sequences published by Brutscher *et al.* in 2009 ((Lescop et al. (2010)). (B) 2D hCconH spectrum collected on the peptidoglycan soluble fragments sample in 11 hours using the pulse sequence published by Wagner *et al.* (Sun et al. (2005)) with 2 DIPSI3 cycles for a total of 15-ms mixing for the ^{13}C-^{13}C transfer. This spectrum correlates the amide proton of a given amino acid to the different side-chain ^{13}C resonances of the preceding amino acid in the peptide stem in the N-terminus direction, offering a clear discrimination between the DAP backbone α and side-chain ϵ sites and thus an identification of DAP residues involved in a cross-link. (C) Superimposition of a 2D ^{13}C-CT-HSQC (red and blue, data collection 2 hours) and a 2D hCcH-TOCSY (black, data collection 6 hours) collected on the peptidoglycan soluble fragments sample. In the constant-time ^{1}H-^{13}C correlation spectrum, resonances in blue and red identify CH groups linked to 1 and 2 aliphatic carbons, respectively. The ^{13}C-^{13}C transfer was allowed during 14 ms in the ^{13}C-edited hCcH-TOCSY experiment. The combination of these two experiments allowed for the specific assignment of each amino acid side-chain ^{1}H and ^{13}C resonances. (D) The ^{1}H-^{15}N INEPT-based correlation spectrum collected in 18 hours on intact *B. subtilis* peptidoglycan in HEPES buffer at pH 7.5 and 30-32°C reveals a signature that is analogous to the pattern obtained from the soluble fragments in panel (A). This spectrum was recorded according to the sequence of Figure 1B at a MAS frequency of 100 kHz.

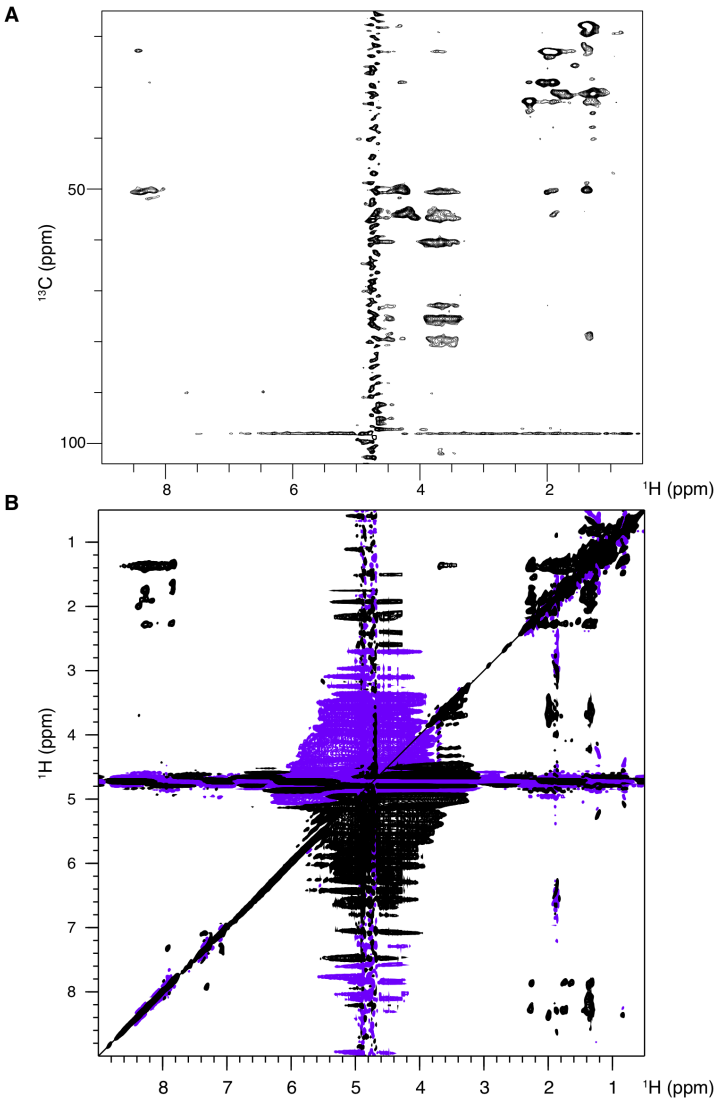

Figure S5: B. subtilis peptidoglycan RFDR spectra. (A) Full-size image of the complete CP-based hChH RFDR spectrum shown in Figure 3B and collected using the sequence depicted in Figure 1D. (B) Full HH-RFDR spectrum collected using the sequence depicted in Figure 1C. This sequence uses a water flip-back pulse to alleviate the problem of water suppression for this peptidoglycan sample prepared in water. Its application results in a ca. 3-4 fold reduction of the solvent signal. Despite the very strong out-of-phase residual solvent signal in the center of the spectrum, key correlations for the assignment can be detected in the amide-to-aliphatic region.

Figure S6: *B. subtilis* peptidoglycan chemical shift resonance assignments.

	Un-crosslinked		Other forms (DAP 3 – 4, crosslinked with D-Ala)		
Residue and position	^{1}H	^{13}C/^{15}N	^{1}H	^{13}C/^{15}N	Comments
GlcNAc					
1	4.48	101.0			
2	3.71	56.0			
3	3.64	73.1			
4	3.56	80.4			
5	3.42	75.7			
6	3.69/3.84	60.7			
HNAc	8.38	123.6			(main component)
HNAc	2.00	23.0			
MurNAc					
1	4.43	103.6			
2	3.71	56.4			
3	3.48	80.6			
4	3.31	73.7			
5	3.81	76.0			
6	3.68/3.82	61.1			
HNAc	7.84	122.6			(very weak)
HNAc	1.90	23.1			
Lac α	4.42	78.6			
Lac βCH_3	1.34	18.4			
L-Ala					
HN	8.24	126.7			
α	4.24	50.9			
β	1.36	17.5			

	Un-crosslinked		Other forms (DAP 3 – 4, crosslinked with D-Ala)		
Residue and position	^{1}H	^{13}C/^{15}N	^{1}H	^{13}C/^{15}N	Comments
D-iGlu					
HN	8.20	126.0			(multiple HN correlations)
α	4.27	55.4			
β	2.08/1.91	29.1			
γ	2.28	32.9			
amidated DAP					
HN	8.23	126.8			(DAP1/2, from tetra-/penta-peptide)
	7.86	131.2			(DAP0, from tri-peptide)
α	4.19	54.8			
β	1.87/1.75	31.1			
γ	1.43	21.6	1.41	22.6	
δ	1.86/1.80	31.1	1.65/1.76	31.9	
ϵ	3.98	53.7	4.09	55.6	
ϵCO$\underline{\mathrm{NH_2}}$	7.05/7.28	108.2	7.29/7.89	109.9	(tentative assignments)
ϵHN			7.81	125.9	
non-amidated DAP					
HN	8.23	126.8			
α	4.17	54.4			
β	1.87/1.75	31.1			
γ	1.42	21.6			
δ	1.78	30.9			
ϵ	3.70	55.5			
D-Ala from tetrapeptide stem or cross-link					
HN	7.91	129.8	7.91	129.8	
α	4.30	50.6	4.30	50.6	
β	1.38	18.0	1.38	18.0	